Open Forum Infectious Diseases

MAJOR ARTICLE

Osteonecrosis of the Femoral Head in People Living With Human Immunodeficiency Virus: A Micro–Computed Tomography Study

Kangpeng Li,[a] Rui Ma,[a] Biao Xu,[a] and Qiang Zhang

National Center for Infectious Diseases, Beijing Ditan Hospital, Capital Medical University, Beijing, China

Background. The incidence of osteonecrosis of the femoral head (ONFH) in people with human immunodeficiency virus (HIV) is 10–100 times higher than that in the general population. However, the specific bone microstructure and extent of damage within the femoral head in PWH are still unclear.

Methods. Femoral head samples were obtained by total hip arthroplasty, micro–computed tomography (micro-CT) was employed to investigate the microstructure of trabecular bone across 4 representative regions within necrotic femoral heads, and quantitative analysis was performed.

Results. On general observation, different degrees of degenerative cartilage, fibrocartilage, hyperplastic bone, and exposed bone were presented alternately, with a "map-like" appearance. On micro-CT, compared with the normal and necrotic areas, the bone volume/tissue volume and bone mineral density of the sclerotic areas were significantly increased, the number of trabeculae was significantly increased, and the gap was smaller ($P < .05$). There was no significant difference in trabecular thickness among the groups ($P < .05$).

Conclusions. The systemic immune syndrome caused by HIV itself may interfere with the normal metabolism of bone, including osteoblasts and osteoclasts, and thus participate in HIV-related ONFH.

Keywords. AIDS; femoral head; HIV; micro-CT; osteonecrosis.

Since the initial report of AIDS in the United States in 1981, humanity has been engaged in a relentless battle against this devastating disease for >4 decades. Despite enduring numerous challenges, remarkable achievements have been made, transforming human immunodeficiency virus (HIV) into a preventable and manageable chronic infectious disease [1]. According to the latest data from The Joint United Nations Programme on HIV/AIDS (UNAIDS) in July 2023, there are currently an estimated 39 million people with HIV (PWH) worldwide, with approximately 1.3 million new cases and 630 000 deaths recorded within the prior year. These figures underscore the persistent prevalence and profound impact of AIDS as one of the most pervasive and detrimental infectious diseases [2].

Osteonecrosis of the femoral head (ONFH) is a pathological process characterized by impaired blood supply, resulting in cellular death and trabecular bone destruction, ultimately leading to deformity and collapse of the femoral head [3]. However, the cause of its occurrence is still unclear. There are 2 mainstream theories. The first is fat embolism caused by excessive glucocorticoid I and alcohol intake, which leads to the death of intramedullary cells. The second is osteonecrosis caused by intraosseous vascular damage and intraosseous hypertension. Since the first reported case of osteonecrosis in a PWH in 1990, this phenomenon has garnered significant attention among clinicians. Although studies have indicated that the incidence of osteonecrosis in the general population ranges from 0.01% to 0.14%, it is notably higher at 1.33%–4.40% among PWH [4, 5]. We suspect that HIV itself is able to participate in ONFH by interfering with bone metabolism. However, current research primarily consists of case reports and retrospective analysis focusing on clinical characteristics alone; thus, there is an urgent need for more comprehensive basic research to elucidate potential pathogenic mechanisms underlying femoral head necrosis in PWH.

Micro–computed tomography (micro-CT) is a computed tomography technique with a spatial resolution ranging from 1 to 10 μm. Utilizing its imaging capabilities, researchers can perform 3-dimensional (3D) reconstruction and morphological analysis of small samples without compromising their internal structure, thereby obtaining accurate parameters describing the

Received 20 September 2023; editorial decision 15 December 2023; accepted 19 December 2023; published online 21 December 2023

[a]K. L., R. M., and B. X. contributed equally to this work and share first authorship.

Correspondence: Qiang Zhang, PhD, National Center for Infectious Diseases, Beijing Ditan Hospital, Capital Medical University, No. 8 Jingshundong Street, Chaoyang District, Beijing 100015, China (zhangqiang202212@163.com).

Open Forum Infectious Diseases®

https://doi.org/10.1093/ofid/ofad660

material's internal architecture. This imaging modality offers numerous advantages including high contrast, ultra-high resolution, real-time imaging capabilities, and multimodal functionality [6]. Due to its ability to clearly distinguish between bone and soft tissue signals, micro-CT is particularly well-suited for bone measurements and has thus found initial applications in the field of bone tissue research. It serves as an invaluable tool for studying changes in bone structure and density during the latent stages of osteoporosis and osteoarthritis animal models. Furthermore, micro-CT is considered a highly suitable method for investigating subtle alterations in 3D bone structure and microstructure.

In this study, micro-CT imaging was employed to examine the bone structure in distinct regions of the necrotic femoral head among PWH, aiming to elucidate the bone microarchitecture within this unique cohort suffering from femoral head necrosis. The findings not only provide valuable guidance for clinical diagnosis and treatment of such patients but also offer insights into potential pathogenic mechanisms underlying femoral head necrosis in individuals with HIV infection.

METHODS

Materials

Fifteen femoral heads were derived from PWH with femoral head necrosis who underwent total hip arthroplasty in the Department of Orthopedics, Beijing Ditan Hospital, Capital Medical University, from September 2019 to September 2021. All patients were diagnosed by X-ray, CT, and magnetic resonance imaging before operation.

Patient Consent

The study protocol was reviewed and approved by the Ethical Committee of Beijing Ditan Hospital affiliated Capital Medical University, and all patients signed informed consent. The ethics lot numbers are Jing Di Lun Ke (2018) number (007)-01 and Jing Di Lun Ke (2018) number (026)-02.

Inclusion Criteria

Inclusion criteria included the following: (1) voluntarily signed informed consent; (2) HIV infection confirmed by enzyme-linked immunosorbent assay and Western blot; (3) orthopedic disease requiring total hip arthroplasty; (4) age 18–60 years; (5) normal results from routine blood analysis, routine urinalysis, liver function tests, and renal function tests; (6) no osteomyelitis (bone infection caused by bacteria or fungi), penetrating wound, or contaminated wound; and (7) no opportunistic infections (eg, hepatitis B, hepatitis C, tuberculosis) or cancer in the past 12 months.

Exclusion Criteria

Exclusion criteria were as follows: (1) female patients who are pregnant or lactating; (2) patients with a fever of >39°C or requiring mechanical ventilation; (3) patients with autoimmune diseases, uncontrolled bleeding diseases, or malignant tumor history; (4) patients with liver and kidney dysfunction or emergency surgery; and (5) participants considered by the investigator to be unsuitable to participate in the study.

Micro-CT Scan

The femoral head specimens were placed in the micro-CT system sample library for fixed scanning, and the scanning slice thickness was 45 μm × 45 μm × 45 μm. The scanning voltage was 80 kV, the scanning current was 450 mA, and the single scanning time was 14 minutes. On this basis, 4 regions of interest were selected according to the calibration procedure of setting the scan results according to the instruction manual: subchondral bone region, necrotic region, sclerotic region, and normal region. GEMIROVIEW software with micro-CT configuration was used for image processing and 3D reconstruction of the region of interest. Bone structural parameters included the following: bone mineral density (BMD); percentage bone volume (BV/TV), ratio of total trabecular bone volume to the sum volume of selected regions; trabecular number (Tb.N), the total number of bone trabeculae identified by gray scale in the selected area; trabecular thickness (Tb.Th), a model-independent thickness 3D structure calculated using the spherical fitting method; and trabecular space (Tb.Sp), the mean value of all bone intertrabecular spaces in the selected area.

Statistical Analysis

SPSS 25.0 statistical software was used for data analysis. For continuous variables with normal distribution and homogeneity of variance, t test was used for comparison between 2 groups, and analysis of variance was used for comparison between multiple groups. To rank the data, the Mann-Whitney U test was used for comparison between groups. Categorical variables were analyzed using the χ^2 test or Fisher exact test, and $P < .05$ was defined as statistically significant.

RESULTS

Baseline Data of the Patients

All femoral head specimens were obtained from PWH undergoing total hip arthroplasty, Association Research Circulation Osseous stage IV. Twelve of 15 patients had undetectable viral loads, and the remaining 3 patients had viral loads <100 copies/mL. All patients were treated with the domestic free drug regimen (tenofovir fumarate/lamivudine/efavirenz) immediately after diagnosis. Detailed demographic information is shown in Table 1, and clinical features are shown in Table 2.

Gross and Coronal Section Manifestations of Femoral Head Specimens From PWH

Gross Appearance

Figure 1 shows that the necrotic femoral heads were mostly hyperplasia and protrusive deformity, with an irregular and

Table 1. Demographic Data of the Patients

Patient No.	Sex	Age, y	BMI, kg/m^2	Route of Infection	Duration of HIV, y	Comorbidity
1	Male	56	18.91	Homosexual intercourse	12	Syphilis, diabetes
2	Male	49	21.33	Homosexual intercourse	8	None
3	Male	38	23.84	Heterosexual intercourse	5	Hepatitis B, syphilis
4	Male	44	21.92	Homosexual intercourse	7	Syphilis
5	Male	51	20.88	Homosexual intercourse	9	Diabetes
6	Male	55	17.35	Heterosexual intercourse	11	Syphilis, HTN
7	Male	35	24.66	Homosexual intercourse	3	Hepatitis B
8	Male	31	19.83	Homosexual intercourse	6	None
9	Male	46	20.22	Heterosexual intercourse	10	None
10	Male	48	22.34	Homosexual intercourse	5	Syphilis
11	Male	52	25.39	Homosexual intercourse	1	None
12	Male	50	18.17	Homosexual intercourse	3	HTN, diabetes
13	Male	46	21.31	Heterosexual intercourse	7	None
14	Male	40	23.56	Homosexual intercourse	5	Syphilis
15	Male	52	22.84	Homosexual intercourse	14	None

Abbreviations: BMI, body mass index; HIV, human immunodeficiency virus; HTN, hypertension.

Table 2. Clinical Characteristics of Patients

Characteristic	Mean ± SD (N = 15)
T-lymphocyte subsets	
CD4 T-lymphocyte count	352.44 ± 125.96
CD8 T-lymphocyte count	804.99 ± 233.46
T-lymphocyte count	1402.73 ± 357.91
CD4/CD8	0.72 ± 0.51
Blood lipids	
Total cholesterol, mmol/L	4.44 ± 0.94
Triglycerides, mmol/L	1.77 ± 1.16
Low-density lipoprotein, mmol/L	2.49 ± 0.34
High-density lipoprotein, mmol/L	1.07 ± 0.11
Blood analysis	
Red blood cells, 10^{12}/L	4.56 ± 0.33
White blood cells, 10^9/L	6.21 ± 1.00
Neutrophils, 10^9/L	2.76 ± 0.89
Lymphocytes, 10^9/L	1.84 ± 0.46
Monocytes, 10^9/L	0.35 ± 0.11
Platelets, 10^9/L	210.27 ± 58.99
Hemoglobin, g/L	137.27 ± 15.10
Liver function tests	
ALT, U/L	23.46 ± 11.96
AST, U/L	21.55 ± 12.97
Albumin, g/L	46.74 ± 2.83
Globulin, g/L	30.12 ± 4.33
Albumin/globulin	1.54 ± 0.29
Electrolyte/renal function	
Calcium, mmol/L	2.31 ± 0.13
Magnesium, mmol/L	0.98 ± 0.08
Phosphorus, mmol/L	0.99 ± 0.15
Urea nitrogen, mmol/L	5.22 ± 1.31
Creatinine, μmol/L	71.30 ± 15.94
Uric acid, μmol/L	381.38 ± 44.16
Glucose, mmol/L	5.19 ± 3.02
eGFR, mL/min	102.78 ± 12.33

Abbreviations: ALT, alanine aminotransferase; AST, aspartate aminotransferase; eGFR, estimated glomerular filtration rate; SD, standard deviation.

uneven surface. Some parts of the cartilage were shrunk and degenerated into yellow-white, some parts were embedded with hyperplastic bone, and the surface of the femoral head was not obviously collapsed. A large number of subchondral bone hyperplasias occurred; the hyperplastic bone was wrapped around the cartilage, and fibrocartilage was formed on the surface of the hyperplastic bone. Different degrees of degenerative cartilage, fibrocartilage, hyperplastic bone, and exposed bone were presented alternately, with a "map-like" appearance. The subchondral bone above the necrotic area of the femoral head was partially exposed and the cartilage was stripped. Subchondral separation was observed in 4 of the 15 patients.

Divisional Representation in the Coronal Plane

As shown in Figure 1, subchondral bone area, most of the cartilage and subchondral bone were well connected. Some of them showed cartilage exfoliation, subchondral bone hyperplasia, wrapping some cartilage; subchondral bone hyperplasia surface formed fibrocartilage, and collapse was not typical. There were some microfractures in the subchondral bone, and subchondral bone hyperplasia surrounding the cartilage was seen.

The necrotic area shows trabecular bone fracture rupture, continuity, and structure disorder; the necrotic area of the femoral head is large, some bone tissue is organized by fibrous tissue, most of the necrotic areas are in the weight-bearing stress area of the femoral head, and the necrotic area shows a semicircle or irregular wedge. It shows yellowish, dark, and reddish color in necrotic areas.

In the sclerotic area, a yellow-white sclerosis zone can be found, and the structure of bone trabeculae is unstable, losing normal mechanics and stress direction. Due to the active bone hyperplasia, the bone trabeculae are widened and

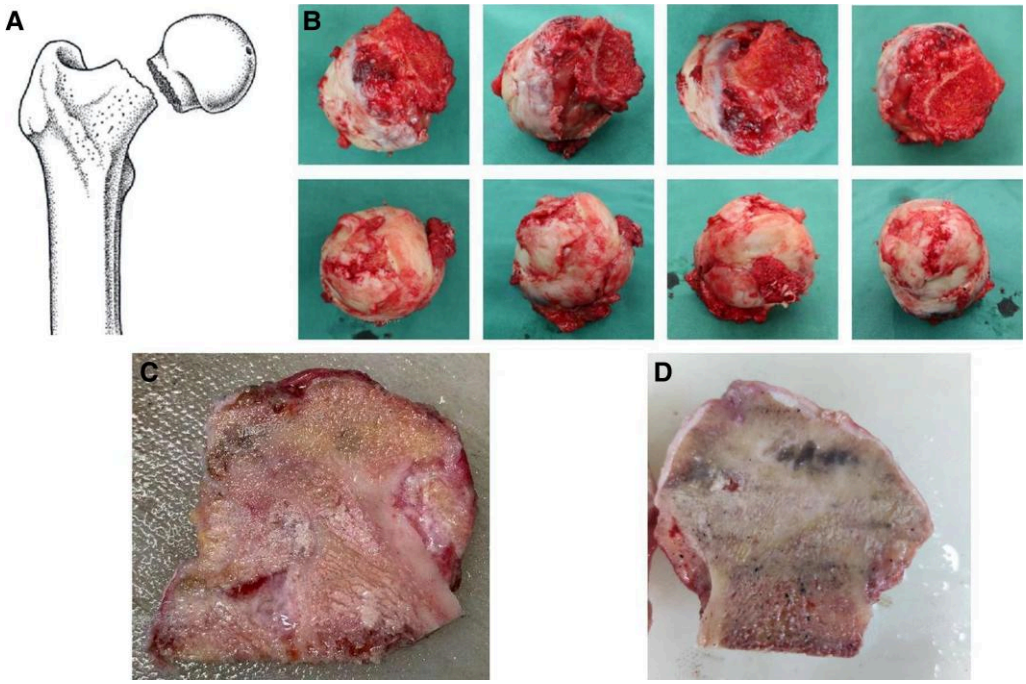

Figure 1. *A*, The pattern of the femoral head was obtained during the operation. *B*, Gross observation of the femoral head in people with human immunodeficiency virus (PWH). *C* and *D*, Coronal view of the femoral head in 2 PWH.

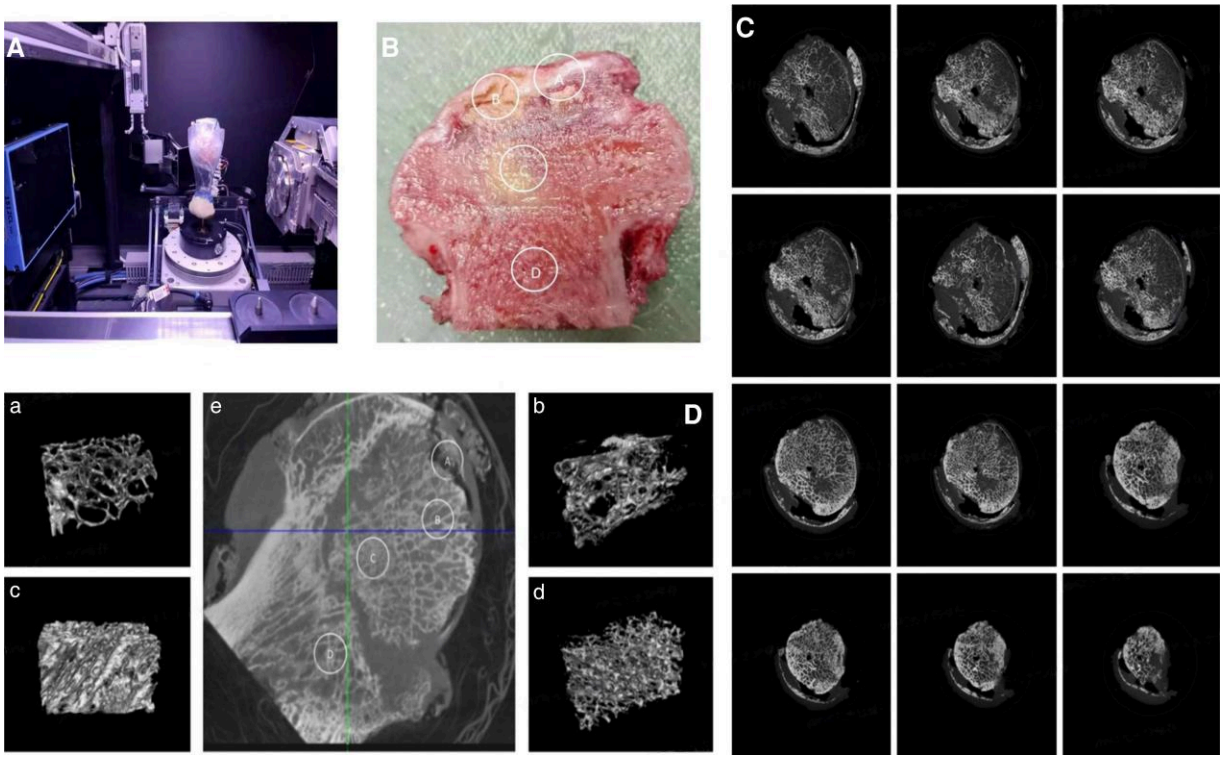

Figure 2. *A*, Micro–computed tomography (micro-CT) instrument. *B*, Schematic diagram of the 4 partitions: Ⓐ subchondral region; Ⓑ necrotic region; Ⓒ sclerotic region; Ⓓ normal region. *C*, Different sections of micro-CT images. *D*, 3D reconstruction of the 4 regions of interest: a, subchondral region; b, necrotic region; c, sclerotic region; d, normal region; e, schematic diagram of the 4 partitions in micro-CT view.

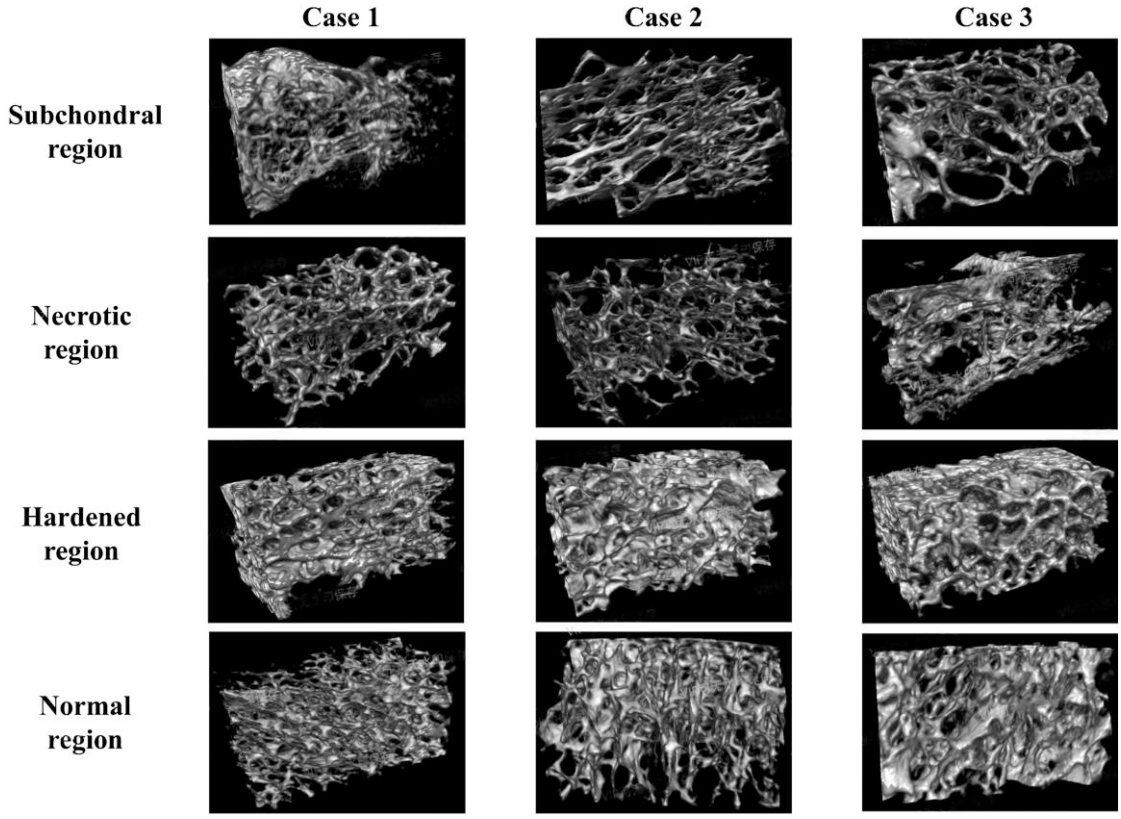

Figure 3. Representative 3D reconstructions of the 4 regions of interest from micro–computed tomography of 3 cases.

thickened, the number is increased, the gap is narrowed, and most of them fuse, so there is a significant difference in the structure and stress direction of bone trabeculae.

In the normal area, the bone trabeculae were arranged according to the normal mechanical structure and stress direction. The structure was normal; the width was evenly distributed; the texture was clear; the bone trabeculae were intact without fracture, sparsity, and hyperplasia; and the color was normal and bright red.

Micro-CT Image Features

In the subchondral area, subchondral bone plate fracture was observed, the longitudinal position reached the calcified cartilage layer, the structure of bone trabeculae was disordered, and the structure of the tide line was blurred. The number of bone trabeculae was variable and the trabecular space was reduced.

The necrotic area showed trabecular bone rupture, continuity damage, structural disorder, some bone tissue organized by fibrous tissue, and loss of trabecular structure.

In the sclerotic zone, the structure of bone trabeculae was disordered, the normal mechanical structure and stress direction were lost, the bone trabeculae were widened and thickened, the number was increased, the gap was narrowed, and most of them fused to form a wide and thick sclerosis band.

In the normal zone, the trabecular bone structure was normal, and the trabecular bone was intact and arranged according to the normal mechanical structure and stress direction. (Figures 2 and 3).

Bone Metrological Analysis

There were significant differences in the measurement parameters of trabecular bone in different regions. Compared with the normal and necrotic areas, the BV/TV and BMD of the sclerotic areas were significantly increased, the number of trabeculae was significantly increased, and the gap was smaller ($P < .05$). There was no significant difference in trabecular thickness among the groups ($P < .05$) (Figure 4).

DISCUSSION

With the introduction and widespread adoption of antiretroviral therapy (ART) in the 1990s, there has been a significant reduction in mortality rates among PWH, accompanied by a substantial increase in life expectancy and enhancement of quality of life. However, both ART and HIV infection itself can give rise to skeletal abnormalities including disturbances in bone metabolism, osteopenia, osteoporosis, fragility fractures, and ONFH. The incidence of ONFH in PWH is 10–100 times higher than that observed in the general population, often leading to walking difficulties and even disability, which imposes a heavy

	BV/TV (%)	Tb.N (N/mm)	Tb.Th (μm)	Tb.Sp (μm)	BMD (mg/cc)
Subchondral region	21.44±3.52	0.94±0.17	399.84±33.36	760±119.82	110.64±18.26
Necrotic region	19.44±5.32	0.65±0.21	365.27±184.68	1013.1±112.4	86.94±10.65
Hardened region	45.9±13.55	1.04±0.08	456.42±93.43	626.07±132.81	182.53±44.91
Normal region	29.93±11.66	0.81±0.12	362.22±99.84	837.2±167.45	152.46±40.86

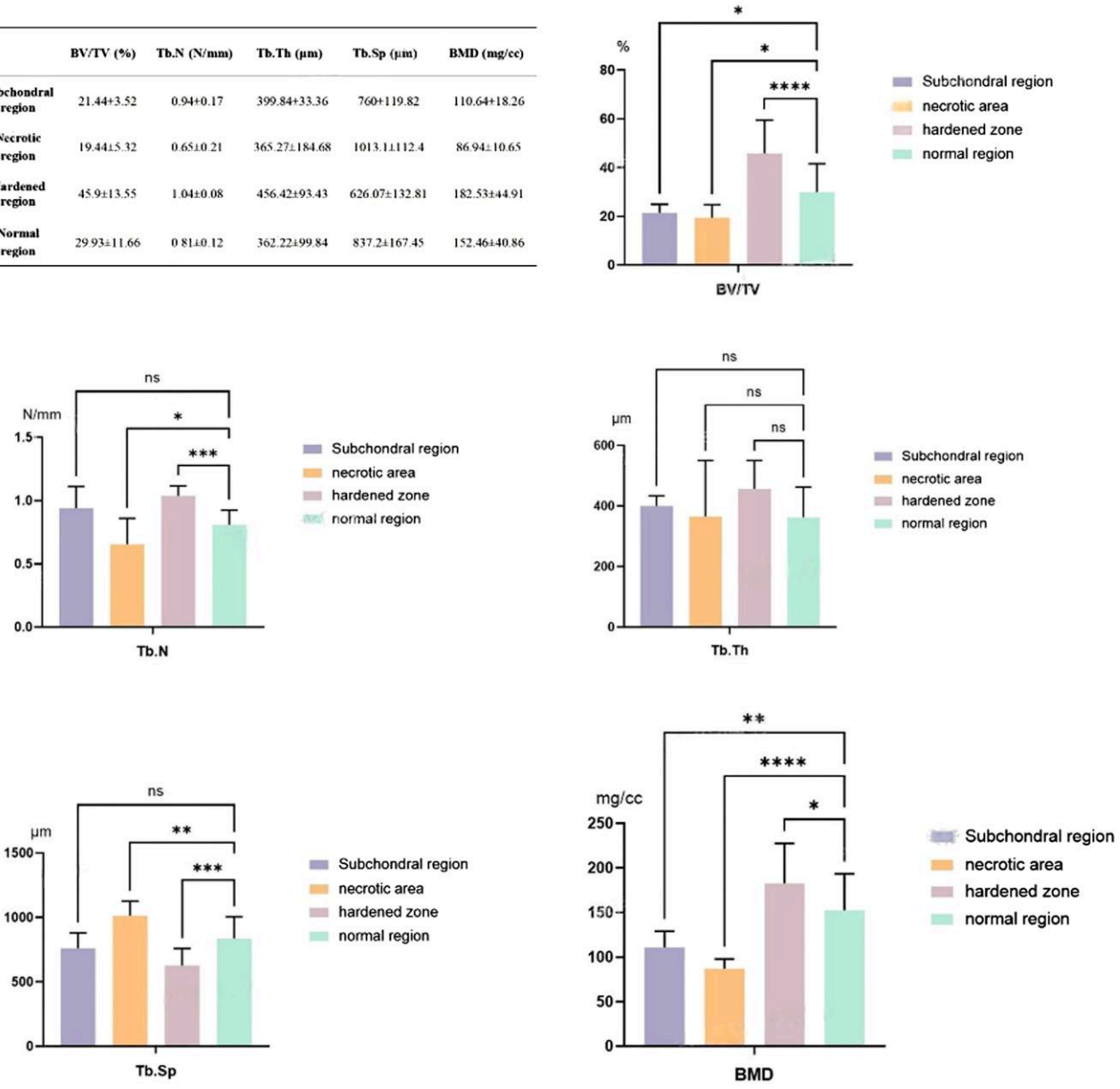

Figure 4. Statistical tables and graphs of the 5 parameters of micro–computed tomography (mean ± SD). *$P < .05$; **$P < .01$; ***$P < .001$; ****$P < .0001$. Abbreviations: BMD, bone mineral density; BV/TV, bone volume/tissue volume; ns, not significant; Tb.N, trabecular number; Tb.Sp, trabecular space; Tb.Th, trabecular thickness.

burden on affected individuals [7, 8]. Furthermore, it is worth noting that most PWH with ONFH seeking treatment at our hospital fall within the age range of 20–50 years; this group represents a valuable labor force for our country. Therefore, it is imperative to elucidate the pathogenesis underlying ONFH development specifically in PWH.

The study of bone can be categorized into 2 dimensions: quantity and quality. The "quantity" of bone refers to its volume or mass, while the "quality" encompasses the characteristics of bone microstructure, collagen composition, and mineralization of the bone matrix. Traditional methods for bone morphometry primarily focus on analyzing 2-dimensional (2D) microscopic images of bone sections, emphasizing the investigation of bone "quantity." However, these methods face challenges in comprehensively assessing aspects such as morphology, density distribution, orientation distribution, and functional mechanical properties related to bone "quality" [9]. Micro-CT technology employs voxels as testing units to reconstruct high-definition 3D trabecular bone structures at a micrometer level. It overcomes limitations associated with destructive and time-consuming staining processes utilized in conventional histomorphology techniques. Micro-CT not only accurately measures overall parameters

related to a specimen's total bone mass but also enables assessment of numerous structural parameters pertaining to bones. This technique provides a novel approach for investigating both the "quantity" and "quality" aspects of bone tissue simultaneously, significantly facilitating research on bone microstructure [10]. To our knowledge, this is the first application of micro-CT in studying ONFH among PWH.

The parameters associated with micro-CT assessment of bone microstructure encompass Tb.Th, Tb.Sp, Tb.N, BV/TV, and BMD. The first 3 indicators primarily reflect the spatial morphological structure of trabecular bone. Decreased Tb.Th and Tb.N along with increased Tb.Sp indicate a higher rate of bone catabolism compared to bone anabolism in osteoporosis. BV/TV directly reflects changes in bone mass by representing the ratio of "bone structure" volume to total volume within the region of interest. BMD represents the density of bone minerals within the region of interest [11]. In this study, there was a significant reduction in BMD within the necrotic area, suggesting that alterations in spatial arrangement and 3D structure of trabecular bones play crucial roles in femoral head collapse. Similar to the necrotic area, subchondral regions exhibited decreased bone mass and density accompanied by reduced space for bones. Conversely, sclerotic areas demonstrated significantly increased BV/TV, Tb.Th, and Tb.N as well as BMD on gross specimens due to active bone repair activity. This indicates a greater emphasis on bone anabolism over catabolism as protective measures against femoral head collapse; however, it also hinders repair reactions from progressing into necrotic areas. We speculate that different areas within ONFH may exhibit varying activities between osteoblasts and osteoclasts.

Studies have demonstrated that the changes in trabecular bone associated with ONFH vary depending on the underlying causes. Alcohol-induced osteonecrosis is characterized by a reduction in trabecular bone mass, while steroid-induced osteonecrosis exhibits more severe morphological destruction of the trabecular structure [12, 13]. In PWH, there were no significant differences observed in trabecular thickness across different regions of the femoral head compared to other causes of femoral head necrosis. This suggests that chronic inflammatory syndrome and persistent immune failure in PWH may interfere with various tissue metabolic responses, including bone tissue metabolism. It is hypothesized that HIV may influence cytokine regulation, thereby affecting mesenchymal stem cell differentiation and apoptosis as well as osteoblast and osteoclast activity, ultimately leading to the development of osteonecrosis. After the start of the repair mode, the mechanical strength of the femoral head decreases, which eventually leads to the change of the spatial structure of the femoral head and the collapse of the femoral head. It is worth mentioning that ART drugs can affect BMD, leading to an increased risk of osteoporotic fractures. Older age, White race, lower current CD4 cell count, and HIV/hepatitis C virus coinfection are independent predictors of fracture risk. However, the relationship between ART and osteonecrosis is still unclear, which needs further study.

Micro-CT offers several advantages over 2D histomorphometry, including the absence of model assumptions, unbiased direct measurement of bone morphological parameters, and nondestructive specimen processing [14]. However, there are certain limitations to consider: (1) Conducting experiments with large samples can be costly; (2) micro-CT lacks sensitivity toward new cartilage and osteoid, making it unsuitable for measuring dynamic parameters related to bone formation, deposition, and absorption; (3) simultaneous scanning of 2 specimens containing metal nails in cancellous bone leads to significant artifacts that greatly affect the surrounding bone tissue analysis [15]; and (4) due to its high-resolution capabilities, micro-CT is currently limited to scientific research applications rather than clinical practice.

This study also has certain limitations. First, the sample size of this study is still relatively small, and we anticipate conducting future studies with larger samples. Second, there was a limited number of patients with a history of alcohol use and glucocorticoid use, which may have potentially confounded the results. Last, all the necrotic femoral head specimens utilized in this study were classified as Association Research Circulation Osseous stage IV; therefore, the internal spatial structure and biomechanical properties of early-stage specimens remain unknown.

CONCLUSIONS

The presence of both necrotic and proliferative repair in femoral heads in PWH was observed. The necrotic femoral head exhibited significant enlargement, with a geographic appearance on the surface; however, evident collapse of the femoral head was not observed. Micro-CT can sensitively and accurately detect 3D structural parameters of trabecular bone, providing insights into the mechanism of osteonecrosis in PWH and offering new guidance for research directions in the treatment of femoral head osteonecrosis.

Notes

Author contributions. All authors contributed to the article and approved the submitted version.

Data availability. The original contributions presented in the study are included in the article. Further inquiries can be directed to the corresponding author.

Potential conflicts of interest. All authors: No reported conflicts.

References

1. Li K, Liu B, Ma R, et al. HIV tissue reservoirs: current advances in research. AIDS Patient Care STDS **2023**; 37:284–96.
2. Balogun K, Slev PR. Towards achieving the end of the HIV epidemic: advances, challenges and scaling-up strategies. Clin Biochem **2023**; 117:53–9.
3. George G, Lane JM. Osteonecrosis of the femoral head. J Am Acad Orthop Surg Glob Res Rev **2022**; 6:e21-00176.
4. Yombi J-C, Vandercam B, Wilmes D, et al. Osteonecrosis of the femoral head in patients with type 1 human immunodeficiency virus infection: clinical analysis and review. Clin Rheumatol **2009**; 28:815–23.

5. Miller KD, Masur H, Jones EC, et al. High prevalence of osteonecrosis of the femoral head in HIV-infected adults. Ann Intern Med **2002**; 137:17–25.
6. Tan J, Labrinidis A, Williams R, et al. Micro-CT-based bone microarchitecture analysis of the murine skull. Methods Mol Biol **2022**; 2403:129–45.
7. Morse CG, Mican JM, Jones EC, et al. The incidence and natural history of osteonecrosis in HIV-infected adults. Clin Infect Dis **2007**; 44:739–48.
8. Borges ÁH, Hoy J, Florence E, et al. Antiretrovirals, fractures, and osteonecrosis in a large international HIV cohort. Clin Infect Dis **2017**; 64:1413–21.
9. Nguyen TV. Common methodological issues and suggested solutions in bone research. Osteoporos Sarcopenia **2020**; 6:161–7.
10. Bouxsein ML, Boyd SK, Christiansen BA, et al. Guidelines for assessment of bone microstructure in rodents using micro-computed tomography. J Bone Miner Res **2010**; 25:1468–86.
11. Rony L, Chappard D. Necrosis of the femoral head, X-ray microtomography (microCT) and histology of retrieved human femoral heads. Morphologie **2021**; 105:134–42.
12. Chen Y, Miao Y, Liu K, et al. Evolutionary course of the femoral head osteonecrosis: histopathological—radiologic characteristics and clinical staging systems. J Orthop Translat **2022**; 32:28–40.
13. Petek D, Hannouche D, Suva D. Osteonecrosis of the femoral head: pathophysiology and current concepts of treatment. EFORT Open Rev **2019**; 4:85–97.
14. Kim Y, Brodt MD, Tang SY, et al. MicroCT for scanning and analysis of mouse bones. Methods Mol Biol **2021**; 2230:169–98.
15. Zheng R-J, Song J-L, Wu X-H, et al. Evaluation of bone formation in neonatal mouse calvariae using micro-CT and histomorphometry: an in vitro study. Acta Histochem **2020**; 122:151614.